DETECTING DAMAGE IN BRIDGES USING VEHICLE INDUCED DYNAMIC RESPONSE: A TIME SERIES ANALYSIS AND ARIMA MODELING APPROACH

Mohammad Abid Hasan*[1] and Shohel Rana[2]

[1] *Lecturer, Dhaka International University, Bangladesh, e-mail: abid.buet17@gmail.com*
[2] *Professor, Bangladesh University of Engineering and Technology, Bangladesh, e-mail: shohel@ce.buet.ac.bd*

***Corresponding Author**

ABSTRACT

Identifying potential damage is crucial in preventing the sudden and premature failure of aging constructions, which has received much attention over the years. This paper suggests an approach where no expensive external excitation equipment is needed. The vehicle-induced dynamic acceleration time series response has been analyzed using a statistical model and statistical distance measurement tool to detect damage to the bridge. The acceleration response depends on many factors, including Vehicle-Bridge Interaction (VBI), vehicle speed and road roughness.

This work is based on a MATLAB and R programming language simulation. The half-car model is used in this simulation to simplify the analysis of the dynamics of the suspension system, as this model has only four degrees of freedom. The car is separated into two parts in this model: the sprung mass (which consists of the vehicle's body and the mass of its occupants) and the unsprung mass (which includes the wheels, tires, and part of the suspension system). The vehicle model is based on the H20-44 truck included in the American Association of State Highway and Transportation Officials (AASHTO) specifications.

A finite element model of a real-life existing bridge, the pre-stressed concrete (PC) bridge named Teesta Bridge, situated in the northern part of Bangladesh, is used in this simulation. The bridge is a supported PC I-girder and consists of five girders with a 200 mm thick deck slab**.** The Vehicle-Bridge Interaction (VBI), vehicle speed, and road roughness all impact the acceleration response data of a bridge. Dynamic bridge structural subsystem and vehicle subsystem models, interaction constraints, and road roughness are all factors in the interaction between automobiles and bridges.

Using the Finite Element Method, mode superposition method, and D'Alembert's principle, two sets of equations of motion are obtained, one for the bridge and the other for the vehicle. Finally, the Newmark-beta method is applied to solve the coupled dynamic problem, and the bridge acceleration time series response is found. Bridge road surface roughness is considered in the analysis as different acceleration responses are generated for different observations due to the presence of randomness. A statistical model, the Autoregressive Integrated Moving Average (ARIMA) model, is used to fit the acceleration time series response originating from healthy and damaged cases. The model parameters are sorted into a matrix called the ARIMA parameter matrix. Then, a statistical distance measurement tool (Mahalanobis Distance) is used here to measure the distance among the ARIMA parameter matrices of healthy and damaged cases, and the presence of any anomaly indicates the existence of damage to the bridge. This proposed technique can identify the existence of damage as well as the location and relative severity of the damage.
The findings of this study demonstrate how the statistical model parameters and statistical distance measurement tools can be utilized to identify damage and assess its relative severity at any point along the bridge span. The effect of varying pavement roughness conditions plays a vital role in this study, as different acceleration time series responses are generated for each observation.

Keywords: *Damage Identification, Vehicle-bridge interaction, Vehicle-induced dynamic acceleration, Newmark's-β Method, Pavement roughness.*

1. INTRODUCTION

Damage is defined as any change to a structure that has a detrimental impact on its functionality or safety, such as material deterioration or boundary condition deterioration. Over time, civil infrastructure, like bridges, sustains damage from both human and natural causes. Because of structural aging, older structures are more vulnerable to natural failure. Environmental effects and the overburdening of the bridge both increase the potential for structural failure. It is crucial to have accurate information about the bridge's health and identify potential harm. Additionally, this allows for better planning of bridge repairs, reducing traffic disturbance and preventing premature collapse. Many bridges have typically been visually inspected regularly (like once a year) to check for damages. Although these techniques essentially work effectively, there are also some crucial downsides. Structural Health Monitoring (SHM) techniques have methodologies. Engineers and asset owners can enhance the systems by using the information supplied by SHM systems. The time series analysis of the dynamic response to detecting damage has received much attention. A combination of time series modeling and outlier detection techniques have been used in most studies focusing on detecting damage using statistical pattern recognition techniques. To detect the damage using the statistical pattern recognition technique, the statistical model parameters have been used as damage-sensitive features. Sohn et al. used a statistical process-controlled technique where the Auto-regressive (AR) model coefficients were used as damage-sensitive features(Sohn et al., 2000). Using X-bar control charts, different levels of damage in a concrete column were identified. Worden et al. and Sohn et al. used Mahalanobis distance to identify structural changes in numerical models and different structures (Farrar et al.; K., 2007). Worden et al. used the transmissibility function, whereas Sohn et al. used AR model coefficients as damage-sensitive features. Omenzetter and Brownjohn used auto-regressive integrated moving average (ARIMA) models to analyze a building's static strain during its construction phase (Omenzetter & Brownjohn, 2006). Although they could detect different structural changes, they could not detect the nature, severity, and location of the structural change. Nair et al. used an auto-regressive moving average (ARMA) model and the first three AR coefficients. Those authors found two different damage localization indices using AR coefficients(Nair et al., 2017).

Zhang proposed another method. The author used a combination of AR and auto-regressive models with exogenous output (ARX models) to identify damage, including the damage location (Zhang et al., 2022). The ARX model's residuals' standard deviation was used as a damage-sensitive feature. A numerical study verified this methodology. In another recent study, Carden and Brownjohn utilized the Auto-regressive moving average (ARMA) model and a statistical pattern classifier that uses the sum of the squares of the residuals of the ARMA model (Peter et al., 2008). However, the authors stated that the vibration data was generated using external excitation and may not apply to structures with only ambient vibration dynamic excitation.

This study proposes a novel data-driven-based technique to detect damage to a prestressed I-girder bridge. A finite element simulation of a prestressed I-girder bridge, whose properties were taken from a real-life existing bridge, is used here. This work uses a statistical model to fit the bridge's dynamic acceleration time series response due to vehicle bridge interaction vibration. The parameters of the best-suited statistical model have been found, and they are fed to a statistical distance measurement tool called Mahalanobis distance to identify the anomalies among the different sets of parameters (Healthy and Damaged cases). However, there are several challenges to be overcome before applying this technique. For instance, environmental and various operational effects may cause significant changes in the structure's dynamic characteristics, and those impacts can mask the actual damage detection techniques. The statistical pattern recognition technique has been very popular as real-life applications have many uncertainties.

2. METHODOLOGY

The methodology in this paper utilizes a Statistical distance measurement tool-based anomaly detection process in conjunction with Auto-regressive integrated moving average (ARIMA) time series modeling. The statistical distance measurement tool that has been used is Mahalanobis distance. The main goal of this paper is to present a modified technique by implementing surface roughness

while constructing the ARIMA models. The randomness in the surface roughness will generate new observations every time the vehicle passes over the bridge. As for the vehicle, a half-car model is used, which is based on the H20-44 truck included in the American Association of State Highway and Transportation Officials (AASHTO) specifications. Moreover, a finite element model is used for the bridge, and the properties are taken from a real-life existing bridge. The whole work is based on a MATLAB and R programming languages simulation. Utilizing the mode superposition method and D'Alembert's principle, two sets of equations of motion are obtained, one for the bridge and the other for the vehicle. Finally, the Newmark-beta method is applied to solve the coupled dynamic problem, and the bridge acceleration response is found. Different damaged case scenarios were created utilizing MATLAB codes, and acceleration responses were generated for healthy and different damaged cases. The difference in acceleration responses for both cases was sought to be detected. In this context, the acceleration time series data were fitted to a statistical model, specifically, the Autoregressive Integrated Moving Average (ARIMA) model. The statistical distances between ARIMA parameter matrices were measured using a statistical distance measurement tool, the Mahalanobis Distance. The anomalous distance was observed to indicate the existence of damage, along with the precise location and severity.

2.1 Time Series Analysis

A time series model is a statistical model used for analyzing and modeling data points collected over some time. It is utilized to identify statistical patterns, trends, and dependencies in time-history data. The current value of the time series is modeled as a linear combination of its past observations. The models can be either univariate, considering only one variable, or multivariate, considering multiple variables. To construct a perfect statistical model that can fit the time series data better compared to other models, we need to observe our time series data first. Based on the data stationarity, a statistical model can be chosen among the Auto-regressive model (AR), Auto-regressive Integrated Moving Average model (ARIMA), or Auto-regressive Moving Average model (ARMA).

2.2 Auto-regressive Integrated Moving Average Model

Vehicle passing over the span is observed and found as stationary time series data. A stationary time series data refers to a time series where the statistical properties remain constant over time. That means the mean, variance, and autocovariance structure of the data do not change their values over time. Using the Augmented Dickey-Fuller (ADF) test, the acceleration time series data is proved to be stationary time series data. The AR or ARIMA model can be utilized for the stationary time series data. AIC (Akaike Information Criterion) and BIC (Bayesian Information Criterion) are used to measure the goodness of a fit. AIC and BIC are used to compare different statistical models. AIC is based on the principles of information theory and is used to evaluate the relative quality of different statistical models. BIC is also the same criterion that is derived from Bayesian principles. Both criteria balance the trade-off between goodness of fit and model complexity. The lower the value of AIC and BIC, the better the statistical fit is. Eventually, an ARIMA statistical model is chosen as this model is more flexible than an AR model. ARIMA model consists of three components: autoregressive (AR) part, differencing (I) part, and moving average (MA) part. Thus, an ARIMA model can be stated as ARIMA (p, d, q) where p indicates AR parameters, d indicates differencing order, and q indicates the MA parameters. ARIMA model can capture both short-term dependencies (MA) and long-term dependencies (AR) in the data. Multiple trial and error processes were performed to determine the parameters of the ARIMA model, and their AIC and BIC values were calculated using MATLAB software. Eventually, for the goodness of fit, the ARIMA (3,0,2) model is chosen to fit the acceleration time series data. The differencing order is found to be zero, again proving the acceleration data's stationarity. The general formula of a pth order ARIMA is defined as follows:

$$y(t) = c + \varphi_1 y(t-1) + \varphi_2 y(t-2) + \ldots + \varphi_p y(t-p) - \theta_1 \varepsilon(t-1) - \theta_2 \varepsilon(t-2) - \ldots - \theta_p \varepsilon(t-q) + \varepsilon(t)$$

Here, y(t) is the time series value at time t, c is a constant, φ is autoregressive (AR) coefficients, θ is moving average (MA) coefficients, and ε(t) is the error term at time t (Chatfield, 2003).

2.3 Anomaly detection

Anomaly detection means the identification of specific data clusters that deviate significantly from the expected behavior of the data clusters. It is a widespread statistical pattern recognition technique. Abnormal data points are assumed to be generated from the erroneous segment of the bridge. In this paper, a statistical distance measurement tool- Mahalanobis distance, is used to identify deviated data clusters and, therefore, the damage in the bridge.

For univariate or 1D data, the anomaly detection process is compared to that of multivariate data. Multiple observations are needed due to the randomness generated from surface roughness. Therefore, different ARIMA models will be created for different observations. Thus, the coefficients found from the ARIMA model will also be different. Five ARIMA parameters will be generated for each observation, and the order of the statistical model is ARIMA (3,0,2). A matrix arrangement of these ARIMA parameters for different observations can be considered an ARIMA parameter matrix, which is multivariate data. As for the multivariate data, the anomaly detection process can be performed using the Mahalanobis distance method.

Mahalanobis squared distance, which will be referred to as Mahalanobis distance from this point.

$$D^2 = (x - \mu)^T \cdot \Sigma^{-1} \cdot (x - \mu)$$

Where:

- x is the p-dimensional data point vector.
- μ is the p-dimensional mean vector of the distribution.
- Σ is the p x p covariance matrix of the distribution.
- Σ-1 is the inverse of the covariance matrix.

The Mahalonobis Distance (MD) will be first applied between two undamaged or healthy ARIMA parameter matrices. Theoretically, the distance would come out to zero, but due to some calculation error, the distance is not exactly zero but close to zero. Then, this MD will be applied to measure the distance between a damaged and healthy case. To apply the MD, the number of observations must be greater than the number of parameters. We have five parameters as we use an ARIMA (3,0,2). So, the minimum number of observations needed is six. So, the order of the ARIMA parameter matrix will be six by five. A sample of this ARIMA parameter is given below:

$$Arima\ Parameter\ Matrix = \begin{vmatrix} \varphi_{11} & \varphi_{12} & \varphi_{13} & \theta_{14} & \theta_{15} \\ \varphi_{21} & \varphi_{22} & \varphi_{23} & \theta_{24} & \theta_{25} \\ \varphi_{31} & \varphi_{32} & \varphi_{33} & \theta_{34} & \theta_{35} \\ \varphi_{41} & \varphi_{42} & \varphi_{43} & \theta_{44} & \theta_{45} \\ \varphi_{51} & \varphi_{52} & \varphi_{53} & \theta_{54} & \theta_{55} \\ \varphi_{61} & \varphi_{62} & \varphi_{63} & \theta_{64} & \theta_{65} \end{vmatrix}$$

2.4 Vehicle Model

A half-car model was considered the design vehicle in this study, as in Fig 1. The underlying reason is to simplify the study, as this vehicle model has only four degrees of freedom. The vehicle's body has two degrees of freedom: vertical vehicle body displacement, y_s and pitching rotation, Θ_s. As for the front and rear wheels, the vertical displacements are y_{t1} and y_{t2}, respectively. Then, using D'Alembert's principle, a set of kinetic equilibrium functions is formulated for each degree of freedom. (Law et al., 2006) (Cavadas et al., 2013; Lu & Liu, 2011).

The equation of motion (EOM) is shown below:

$$m_s\ddot{y}_s + c_{s1}(\dot{y}_s - \dot{y_{t1}} + \dot{\theta}a_1) + c_{s2}(\dot{y}_s - \dot{y}_{t2} - \dot{\theta}a_2) + k_{s1}(y_s - y_{t1} + \theta a_1) + k_{s1}(y_s - y_{t2} - \theta a_2) = 0 \quad (1)$$

$$J\ddot{\theta} + k_{s1}a_1(y_s - y_{t1} + \theta a_1) - k_{s2}a_2(y_s - y_{t2} - \theta a_2) + c_{s1}a_1(\dot{y}_s - \dot{y}_{t1} + \dot{\theta}a_1) - c_{s2}a_2(\dot{y}_s - \dot{y}_{t2} - \dot{\theta}a_2) = 0 \quad (2)$$

$$m_{t1}\ddot{y}_{t1} - k_{s1}(y_s - y_{t1} + \theta a_1) - c_{s1}(\dot{y}_s - \dot{y}_{t1} + \dot{\theta}a_1) + k_{t1}(y_{t1} - y_{c1}) = 0 \quad (3)$$

$$m_{t2}\ddot{y}_{t2} - k_{s2}(y_s - y_{t1} + \theta a_2) - c_{s2}(\dot{y}_s - \dot{y}_{t2} + \dot{\theta}a_2) + k_{t2}(y_{t2} - y_{c2}) = 0 \quad (4)$$

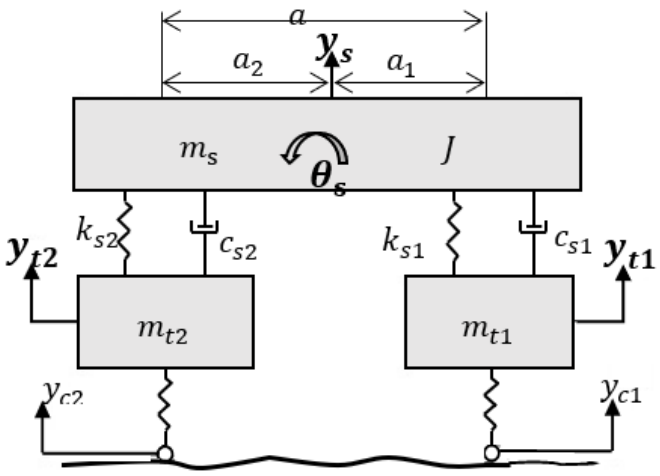

Fig. 1. Half-car vehicle model.

M_s represents the vehicle body and frame mass, basically the vehicle's sprung mass. Then m_{t1} m_{t2} represent the mass of the axle between the front and back wheelset and tires; c_{s1}, c_{s2}, k_{s1}, k_{s2} are the suspension damping and stiffness between the sprung and unsprung mass segment of the vehicle. Then k_{t1} and k_{t2} are the stiffness of the front and rear wheel tires, respectively. The front and rear wheel distance from the vehicle's centre of gravity is denoted using a_1 and a_2, respectively, which gives us the value of $a = a_1 + a_2$: distance between the front and rear wheel. The vertical displacement on the point of bridge contact with the front and rear wheels is denoted using y_{c1} and y_{c2}, where the vertical displacement between the sprung and unsprung mass of the vehicles is represented using y_{t1} and y_{t2}. A new equation (5) is derived using the equations above (1-4).

$$[M_v]\{\ddot{y}_v(t)\} + [C_v]\{\dot{y}_v(t)\} + [K_v]\{y_v(t)\} = \{F_v\} \tag{5}$$

Where $[M_v]$, $[C_v]$, $[K_v]$ are the mass, damping, and stiffness matrices of the vehicle, respectively, $\{y_v(t)\}$ is the DOF vector, and $\{F_v\}$ represents the exciting force for the vehicle vibration. Here,

$$[M_v] = \begin{bmatrix} m_s & 0 & 0 & 0 \\ 0 & J & 0 & 0 \\ 0 & 0 & m_{t1} & 0 \\ 0 & 0 & 0 & m_{t2} \end{bmatrix} \tag{6}$$

$$\{y_v\} = \begin{Bmatrix} y_s \\ \theta \\ y_{t1} \\ y_{t2} \end{Bmatrix} \tag{7}$$

$$[K_v] = \begin{bmatrix} k_{s1} + k_{s2} & k_{s1}a_1 - k_{s2}a_2 & -k_{s1} & -k_{s2} \\ k_{s1}a_1 - k_{s2}a_2 & k_{s1}a_1^2 + k_{s2}a_2^2 & -k_{s1}a_1 & k_{s2}a_2 \\ -k_{s1} & -k_{s1}a_1 & k_{s1} + k_{t1} & 0 \\ -k_{s2} & k_{s2}a_2 & 0 & k_{s2} + k_{t2} \end{bmatrix} \tag{8}$$

$$[C_v] = \begin{bmatrix} c_{s1} + c_{s2} & c_{s1}a_1 - c_{s2}a_2 & -c_{s1} & -c_{s2} \\ c_{s1}a_1 - c_{s2}a_2 & c_{s1}a_1^2 + c_{s2}a_2^2 & -c_{s1}a_1 & c_{s2}a_2 \\ -c_{s1} & -c_{s1}a_1 & c_{s1} & 0 \\ -c_{s2} & c_{s2}a_2 & 0 & c_{s2} \end{bmatrix} \tag{9}$$

2.5 Model of Bridge

This study uses a finite element model of a bridge for the simulation. The properties of the finite element model are taken from a real-life bridge, the pre-stressed concrete (PC) Bridge named Teesta Bridge, situated in the northern part of Bangladesh. The bridge is a supported PC I-girder and consists of five girders with a 200 mm thick deck slab. Each span of the bridge is 50 m. A single lane of the bridge subjected to one vehicle is considered for the finite element modelling. The span of the bridge is 50 m. The flexural rigidity (EI) and mass of the bridge girder are 6.96×10^{10} Nm^2 and 6818.5 kg/m, respectively. 5% modal damping is assumed for the bridge for all the modes. The mass per unit length of span is defined by m. The EOM for the bridge is formulated as in Eq. (10).

$$[M_b]\{\ddot{y}_b(t)\} + [C_b]\{\dot{y}_b(t)\} + [K_b]\{y_b(t)\} = \{F_b(x,t)\}\delta(x - vt) \quad (10)$$

Where $[M_b]$, $[C_b]$, $[K_b]$ are the mass, damping, and stiffness matrices of the bridge, Fb(x,t) denotes the coupled forces on the bridge, and the vertical bridge displacement at nodal points at time t is represented by $\{y_b(t)\}$, and δ defines the Dirac function.

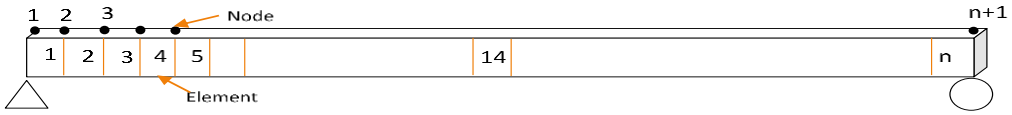

Fig. 2. FE model of the bridge.

Some low-order modes of vibration mainly control the dynamic response of a structure. A few lowest modes are usually enough to find a satisfactory result in implementing the superposition method. As a result, the computational efficiency will be achieved. The finite element modeled bridge is then segmented into 'N' elements; therefore, the degrees of freedom (DOF) are taken as 'N.' The number of modes used in this simulation affects the findings to a great extent. Therefore, the number of the modes taken into consideration is 2. As shown in Eq, the bridge displacement can be determined using the mode superposition method.

$$y_b(x,t) = \{\ddot{y}_b(t)\} = \sum_{i=1}^{N} \{\varphi_i\}\eta_i(t) = [\varphi]\{\eta(t)\}$$

$\{\varphi i\}$ and $\eta i(t)$ are the vibration mode shape of the bridge and modal coordinates, respectively. The EOM of the bridge in modal coordinate is obtained by substituting Eq. (11) into Eq. (10) as shown in Eq. (12). Multiplying both sides of Eq. (12) by $\{\varphi_n\}^T$, Eq. (13) has been obtained and after implementing modal orthogonality principal (Chopra, A.K., 2007)

$$\{\varphi_n\}^T[M]\{\varphi_i\} = 0,\ \{\varphi_n\}^T[M]\{\varphi_n\} = M_n\ ;\ \{\varphi_n\}^T[K]\{\varphi_i\} = 0, \{\varphi_n\}^T[K]\{\varphi_n\} = K_n$$

The *N* uncoupled second-order differential equations in modal coordinates have been obtained as in EQ. (14).

$$[M_b][\varphi]\{\ddot{\eta}(t)\} + [C_b][\varphi]\{\dot{\eta}(t)\} + [K_b][\varphi]\{\eta(t)\} = -\{F_b(x,t)\}\delta(x - vt)$$

$$\{\varphi_n\}^T[M_b][\varphi]\{\ddot{\eta}(t)\} + \{\varphi_n\}^T[C_b][\varphi]\{\dot{\eta}(t)\} + \{\varphi_n\}^T[K_b][\varphi]\{\eta(t)\} = -\{\varphi_n\}^T\{F_b(x,t)\}\delta(x - vt)$$

$$\ddot{\eta}_n(t) + 2\zeta_n\omega_n\dot{\eta}_n(t) + \omega_n^2\eta_n(t) = -\frac{1}{M_n}\{\varphi_n\}^T\{F_b(x,t)\}\delta(x - vt)$$

Where ωn, Mn, ζn are the natural frequency of vibration mode, modal mass, and modal damping ratio of nth mode, respectively; if x=vt, δ(x-vt)=1 else 0. The Eigen-value problem governing this *N* DOF linear dynamic system can be expressed as in Eq. (16). This Eigen-value problem of the bridge is solved using Eigen-solution for determining the natural frequencies and vibration mode shapes of the bridge.

$$\left[[K_b] - \omega_r^2[M_b]\right]\{\phi_r\} = \{0\}$$

2.6 Vehicle Bridge Interaction

Two separate sets of differential equations have now been developed. One is for the vehicle, as in Eq. (5), and the other is for the bridge, as in Eq. (14). The matrices resulting from two sets of differential equations are coupled to establish interaction between vehicle and bridge system responses. The compatibility conditions are applied at the contact points to develop interaction between the vehicle and the bridge sub-systems, and the coupled equation of motions is formulated. The effect of pavement roughness is included here since both the pavement roughness and the bridge displacement cause wheel displacement. $Y_{b1}(x1,t)$ and $Y_{b2}(x2,t)$ are the bridge displacement responses at the front and rear wheel contact points. As per the compatibility condition, the front and rear wheel vertical displacements, y_{c1} and y_{c2}, respectively, are calculated as in Eqs. (16) and (17). Also, the contact forces on the bridge consist of the weight of the vehicle and wheel body and the elastic forces as calculated in Eqs. (18) and (19). These forces result in the coupling between the bridge and vehicle vibration. The coupled form of the vehicle bridge model is depicted in Fig. 3.

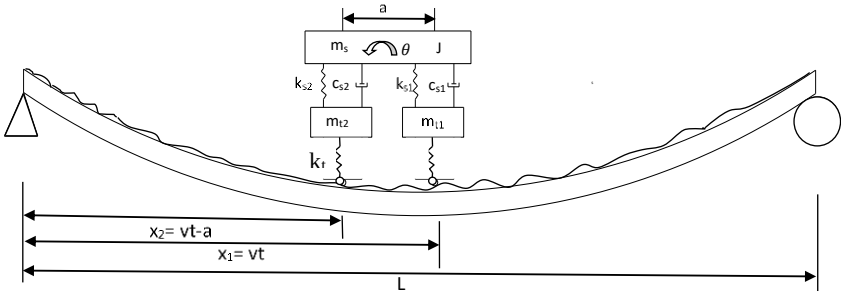

Fig. 3. The model of coupled vehicle-bridge vibration.

$$y_{c1} = y_b(x_1,t) + r(x_1) = \sum_{n=1}^{N} \varphi_n(x_1)\eta_n(t) + r_1 = \sum_{n=1}^{N} \varphi_{1n}\eta_n(t) + r_1 \qquad (16)$$

$$y_{c2} = y_b(x_2,t) + r(x_2) = \sum_{n=1}^{N} \varphi_n(x_2)\eta_n(t) + r_2 = \sum_{n=1}^{N} \varphi_{2n}\eta_n(t) + r_2 \qquad (x_2 = x_1 - a) \qquad (17)$$

$$F_1(x_1,t) = W_1 - K_{t1}(y_{t1} - y_{c1}) \qquad (18)$$

$$F_2(x_2,t) = W_2 - K_{t2}(y_{t2} - y_{c2}) \qquad (19)$$

Where r1 and r2 are the deck surface roughness and φ1 and φ2 are the mode shape values of nth mode at the front and rear wheel contact points, respectively. F1(x1,t) and F2(x2,t) are the point forces at the wheel contact points; W is the static load comprising sprung and un-sprung weights. Here, the coupling has been done within matrix format by applying the compatibility conditions to equations (3-4) and (12). We are applying the above conditions to Eqs. (3-4), Eqs. (20-21) are derived. Replacing Fi(x,t) from Eqs. (18-19) into Eq. (14), and after rearranging, Eq. (24) is derived. Finally, Eqs. (1-2) and (20-22) are converted to a matrix representation as in Eq. (23), which is the coupled matrix formulation for both the vehicle and the bridge subsystems interacting together.

$$m_{t1}\ddot{y}_{t1} - k_{s1}(y_s - y_{t1} + \theta a_1) - c_{s1}(\dot{y}_s - \dot{y}_{t1} + \dot{\theta}a_1) + k_{t1}\left\{y_{t1} - \left(\sum_{n=1}^{N} \varphi_{1n}\eta_n(t) + r_1\right)\delta_1\right\} = 0 \qquad (20)$$

$$m_{t2}\ddot{y}_{t2} - k_{s2}(y_s - y_{t1} + \theta a_2) - c_{s2}(\dot{y}_s - \dot{y}_{t2} + \dot{\theta}a_2) + k_{t2}\left\{y_{t2} - \left(\sum_{n=1}^{N} \varphi_{2n}\eta_n(t) + r_2\right)\delta_2\right\} = 0 \qquad (21)$$

$$\frac{a_2\varphi_{1n}\delta_1 + a_1\varphi_{2n}\delta_2}{a} m_s\ddot{y}_s + \frac{\varphi_{1n}\delta_1 - \varphi_{2n}\delta_2}{a} J\ddot{\theta} + \varphi_{1n}\delta_1 m_{t1}\ddot{y}_{t1} + \varphi_{2n}\delta_2 m_{t2}\ddot{y}_{t2} + \ddot{\eta}_n + 2\zeta_n\omega_n\dot{\eta}_n + \omega_n^2\eta_n =$$
$$-(\varphi_{1n}W_1\delta_1 + \varphi_{2n}W_2\delta_2) \qquad (22)$$

$$[M(t)]\{\ddot{Y}\} + [C(t)]\{\dot{Y}\} + [K(t)]\{Y\} = \{Q(t)\} \qquad (23)$$

Here, [M(t)], [C(t)], and [K(t)] represent (n+4) orders coupled with time-dependent mass, damping, and stiffness matrices of the vehicle and the bridge together, which are formulated in Eqs. (24-26); {Y} represents (n+4) order displacement vector consisting of the modal response of the bridge combined with the vehicle response. {Q(t)} represents (n+4) order force vector as shown in Eq. (27). By solving Eq. (23), vehicle responses can be obtained directly from the solution, and bridge responses are calculated using Eq. (11).

$$[M(t)] = \begin{bmatrix} m_s & 0 & 0 & 0 & 0 & 0 & \dots & 0 \\ 0 & J & 0 & 0 & 0 & 0 & \cdots & 0 \\ 0 & 0 & m_{t1} & 0 & 0 & 0 & \cdots & 0 \\ 0 & 0 & 0 & m_{t2} & 0 & 0 & \cdots & 0 \\ \frac{a_2\varphi_{11}\delta_1 + a_1\varphi_{21}\delta_2}{a} m_s & \frac{\varphi_{11}\delta_1 - \varphi_{21}\delta_2}{a} J & \varphi_{11}\delta_1 m_{t1} & \varphi_{21}\delta_2 m_{t2} & 1 & 0 & \cdots & 0 \\ \frac{a_2\varphi_{12}\delta_1 + a_1\varphi_{22}\delta_2}{a} m_s & \frac{\varphi_{12}\delta_1 - \varphi_{22}\delta_2}{a} J & \varphi_{12}\delta_1 m_{t1} & \varphi_{22}\delta_2 m_{t2} & 0 & 1 & \cdots & 0 \\ \vdots & \vdots & \vdots & \vdots & \vdots & \vdots & \cdots & \vdots \\ \frac{a_2\varphi_{1n}\delta_1 + a_1\varphi_{2n}\delta_2}{a} m_s & \frac{\varphi_{1n}\delta_1 - \varphi_{2n}\delta_2}{a} J & \varphi_{1n}\delta_1 m_{t1} & \varphi_{2n}\delta_2 m_{t2} & 0 & 0 & 0 & 1 \end{bmatrix} \quad (24)$$

$$[K(t)] = \begin{bmatrix} k_{s1}+k_{s2} & k_{s1}a_1 - k_{s2}a_2 & -k_{s1} & -k_{s2} & 0 & 0 & \cdots & 0 \\ k_{s1}a_1 - k_{s2}a_2 & k_{s1}a_1^2 + k_{s2}a_2^2 & -k_{s1}a_1 & k_{s2}a_2 & 0 & 0 & \cdots & 0 \\ -k_{s1} & -k_{s1}a_1 & k_{s1}+k_{t1} & 0 & -k_{t1}\varphi_{11}\delta_1 & -k_{t1}\varphi_{12}\delta_1 & \cdots & -k_{t1}\varphi_{1n}\delta_1 \\ -k_{s2} & k_{s2}a_2 & 0 & k_{s2}+k_{t2} & -k_{t2}\varphi_{21}\delta_2 & -k_{t2}\varphi_{21}\delta_2 & \cdots & -k_{t2}\varphi_{2n}\delta_2 \\ 0 & 0 & 0 & 0 & \omega_1^2 & 0 & \cdots & 0 \\ 0 & 0 & 0 & 0 & 0 & \omega_2^2 & \cdots & 0 \\ \vdots & \vdots & \vdots & \vdots & \vdots & \vdots & \cdots & \vdots \\ 0 & 0 & 0 & 0 & 0 & 0 & \cdots & \omega_n^2 \end{bmatrix} \quad (25)$$

$$[C(t)] = \begin{bmatrix} c_{s1}+c_{s2} & c_{s1}a_1 - c_{s2}a_2 & -c_{s1} & -c_{s2} & 0 & 0 & \cdots & 0 \\ c_{s1}a_1 - c_{s2}a_2 & c_{s1}a_1^2 + c_{s2}a_2^2 & -c_{s1}a_1 & c_{s2}a_2 & 0 & 0 & \cdots & 0 \\ -c_{s1} & -c_{s1}a_1 & c_{s1} & 0 & 0 & 0 & \cdots & 0 \\ -c_{s2} & c_{s2}a_2 & 0 & c_{s2} & 0 & 0 & \cdots & 0 \\ 0 & 0 & 0 & 0 & 2\zeta_1\omega_1 & 0 & \cdots & 0 \\ 0 & 0 & 0 & 0 & 0 & 2\zeta_2\omega_2 & \cdots & 0 \\ \vdots & \vdots & \vdots & \vdots & \vdots & \vdots & \cdots & \vdots \\ 0 & 0 & 0 & 0 & 0 & 0 & 0 & 2\zeta_n\omega_n \end{bmatrix} \quad (26)$$

$$\{Q(t)\} = \begin{Bmatrix} 0 \\ 0 \\ k_{t1}r_1\delta_1 \\ k_{t2}r_2\delta_2 \\ -(\varphi_{11}W_1\delta_1 + \varphi_{21}W_2\delta_2) \\ -(\varphi_{12}W_1\delta_1 + \varphi_{22}W_2\delta_2) \\ \vdots \\ -(\varphi_{1n}W_1\delta_1 + \varphi_{2n}W_2\delta_2) \end{Bmatrix} \quad (27) \qquad \{Y(t)\} = \begin{Bmatrix} y_s(t) \\ \theta \\ y_{t1}(t) \\ y_{t2}(t) \\ \eta_1(t) \\ \eta_2(t) \\ \vdots \\ \eta_n(t) \end{Bmatrix} \quad (28)$$

3. BRIDGE DECK SURFACE ROUGHNESS MODELLING

The vehicle's wheels are assumed to remain in contact with the bridge deck. Therefore, at the contact points, the displacement of the wheels equals that of the bridge deck with surface roughness. The surface roughness also plays a vital role in stimulating vehicle vibrations. The bridge deck surface roughness is simulated theoretically herein. The table shows that artificial surface roughness representing the Class A-B profile has been generated according to ISO 8608 classification [43,44]. 1 using the Eq. (29).

$$r(x) = \sum_{i=0}^{N} \sqrt{\Delta n}.2^{k}.10^{-3}.\left(\frac{n_0}{i.\Delta n}\right).cos(2\pi.i.\Delta n.x + \varphi_i) \qquad (29)$$

Where r(x) is the elevation/roughness of the road profile; L represents the length of the bridge, and B is the sampling interval; x represents the abscissa variable from 0 to L; Δn = 1/L;nmax=1/B; n0= 0.1 cycles/m; k denotes a constant value depending upon ISO road roughness classification which varies from 3 to 9, corresponding to the road roughness profiles from class A to class H. Also, φi represents a random phase angle within the 0-2π range, which follows a uniform probabilistic distribution. Here, Fig. 4 demonstrates a typical Class A-B bridge deck roughness profile generated using Eq. (29). (Agostinacchio et al., 2014; Múčka, 2017)

Upper Limit	Lower Limit	k	Quality
A	B	3	Very Good
B	C	4	Good
C	D	5	Average
D	E	6	Poor
E	F	7	Very Poor

Table 1. Road Roughness Classification

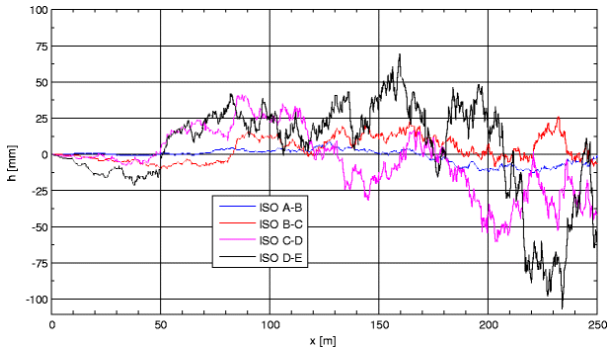

Fig. 4. Typical bridge deck surface roughness.

4. DAMAGE CASES

This paper considers three types of damage cases utilizing MATLAB codes. Artificial damage is created by reducing the bridged element's stiffness. Different types of damage severity are created depending on the degree of stiffness reduction. The damage will be identified using the anomaly detection technique concerning location and severity.

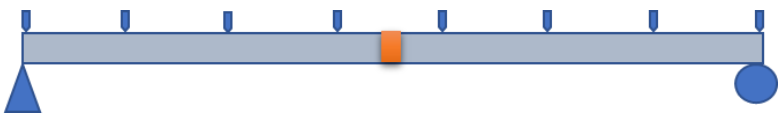

Fig. 5. Damage condition one at mid-point(D1)

Fig. 6. Damage condition two at one-fourth distance from the support (D2)

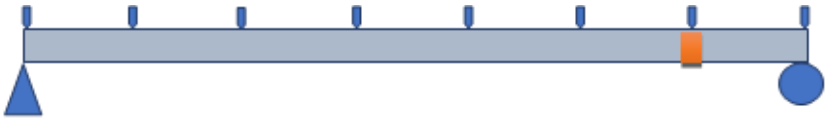

Fig. 6. Damage condition three at a three-fourth distance from the support (D3)

5. IDENTIFICATION OF THE EXISTENCE OF THE DAMAGE

To identify the existence of the damage, only one sensor is required. For this purpose, for a specific damage severity (40%), an acceleration sensor is placed in our simulation at the middle of the span for different damage cases. Then, the ARIMA parameters are extracted for all the cases for that specific location's acceleration time series data. This process is repeated six times as randomness requires different observation data. Then, the ARIMA parameter matrixes are generated for healthy and different damage cases. The Mahalanobis distances of the ARIMA parameter matrix have been measured among the healthy and damaged cases and plotted against the observations.

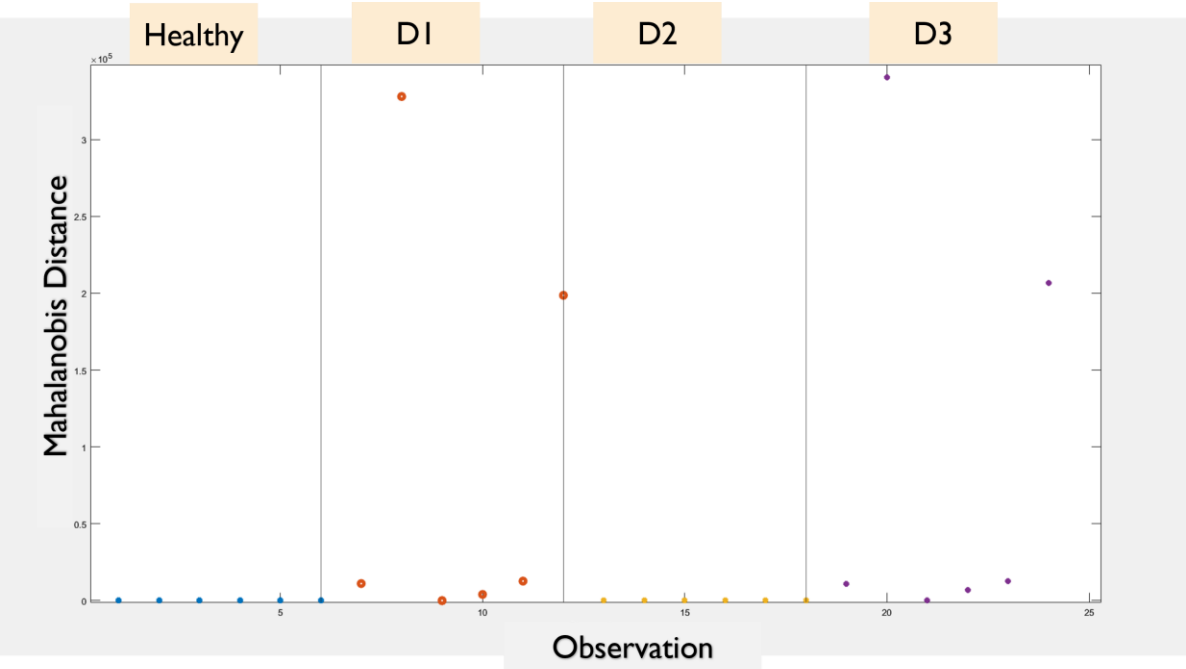

Fig. 7. Observation vs. Mahalanobis Distance to identify the existence of the damage

6. IDENTIFICATION OF THE LOCATION OF THE DAMAGE

We need more than one sensor installed on the bridge span to find the damaged location. The ARIMA parameter matrix will be performed as a damage index for a fixed damage severity (40%) difference of Mahalanobis distance between healthy and damaged cases. The first step in identifying damage on the bridge span is to identify the location of the damaged element. For this purpose, multiple acceleration sensors are placed at different span locations. In this simulation work, eight acceleration sensors were used to identify the location of damage that had been done artificially at a specific position utilizing the MATLAB code. At one-fourth of the distance from the support, this artificial damage has been done, and the damage case is called D2. ARIMA parameter matrixes are generated for all these positions for healthy and damaged cases. Then, the sum of the Mahalanobis distances is measured among the ARIMA parameter matrix to show the anomalies.

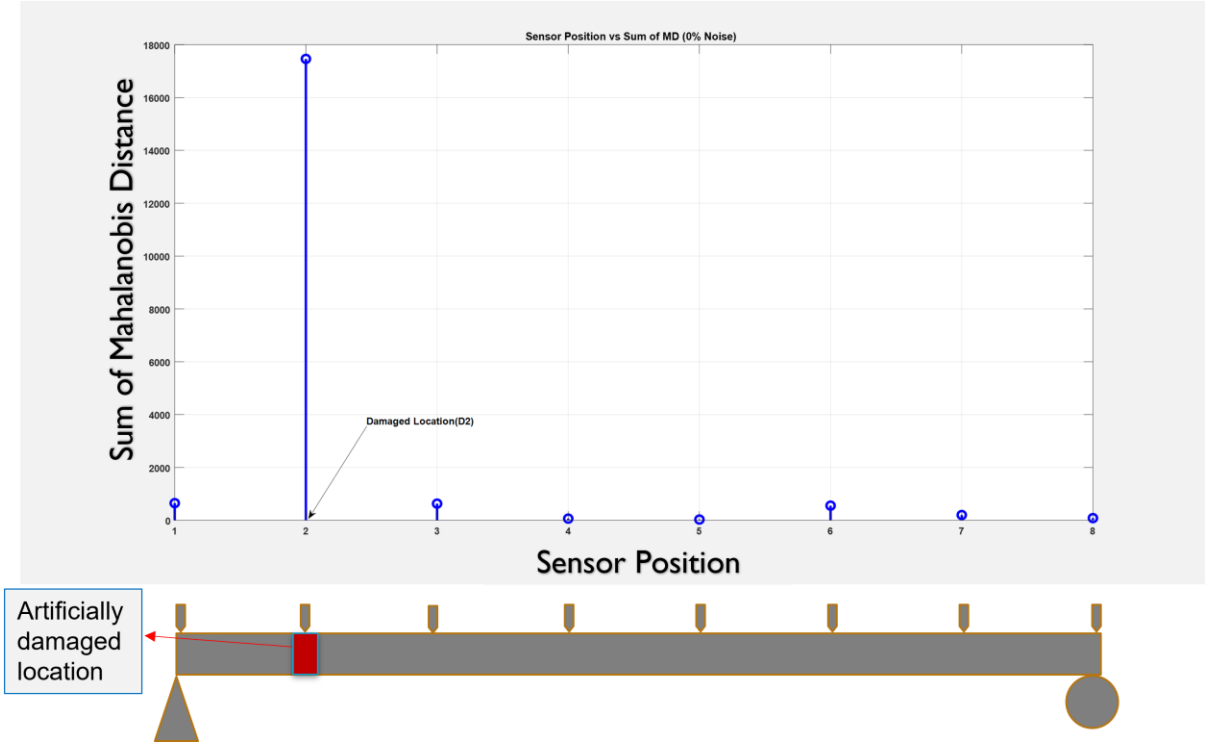

Fig. 8. Sensor Position vs Sum of Mahalanobis Distance

7. EFFECT OF DIFFERENT DAMAGE SEVERITY OF DAMAGE INDEX

After identifying the damaged location using the Sum of Mahalanobis distance as the damage index, the impact of damage severity on the damage index is found; the same procedures are followed here except that various damage severity cases are considered here. The following graph indicates that the higher the damage severity, the higher the damage index. This indication further proves the applicability of this damage identification technique.

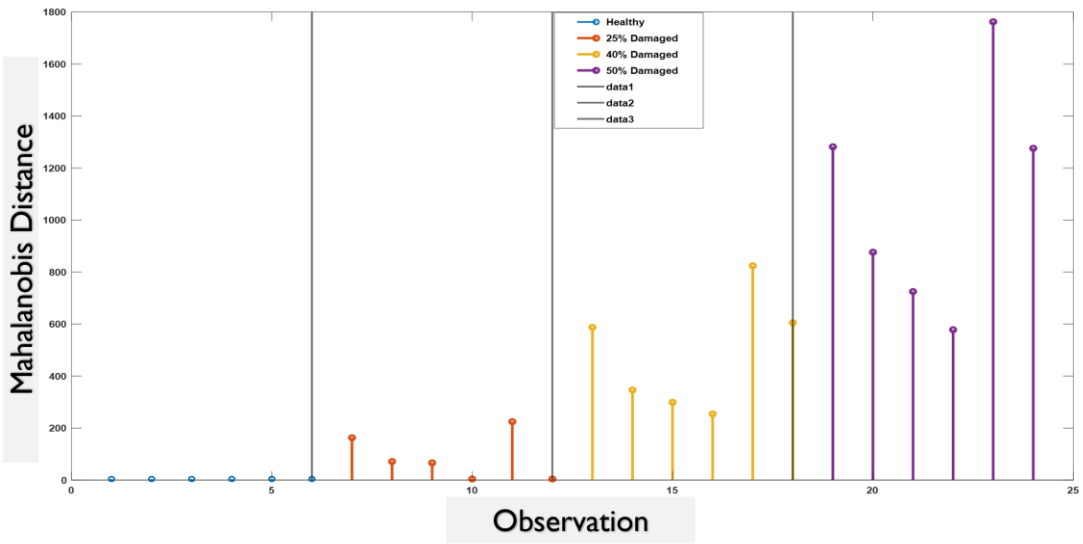

Fig. 9. Observation vs. Mahalanobis Distance for different damage severity

8. CONCLUSIONS

An existing structure's safety is crucial for the clients' and occupancies' safety. It has been said that typical damage identification processes are obsolete and less accurate, and we must search for a smart technique. This paper develops the damage detection method based on the vehicle-induced bridge dynamic acceleration time series response of the bridge derived from the vehicle-bridge interaction (VBI). Vehicle-bridge interaction modeling is a complex process that involves several factors such as bridge finite element model, half-car vehicle model, pavement deck roughness, vehicle speed, and interaction between the vehicle and the bridge at the contact point. After fitting the acceleration response for different observations into a statistical model (ARIMA), the ARIMA parameters were extracted and sorted into a matrix called the ARIMA parameter matrix. Later, a statistical distance measurement tool (Mahalanobis distance) is used to detect the anomalies among healthy and damaged ARIMA parameter matrixes. The suggested technique made it possible to track damage over time by determining its location and relative severity. Also, this work proved less susceptible to noise, making it even more reliable. The application of this technique to naturally damaged bridges will be the focus of this study's future efforts.

ACKNOWLEDGEMENTS

I am highly indebted to my undergraduate supervisor, Dr Shohel Rana. Without his help, I could not have written this paper.

REFERENCES

Akiyama, H., Fukada, S., & Kajikawa, Y. (2007). Numerical study on the vibrational serviceability of flexible single-span bridges with different structural systems under traffic load. *Structural Engineering International*, *17*(3), 256-263.

Amezquita-Sanchez, J. P., & Adeli, H. (2016). Signal processing techniques for vibration-based health monitoring of intelligent structures. *Archives of Computational Methods in Engineering*, *23*(1), 1-15.

Cai, C. S., Shi, X. M., Araujo, M., & Chen, S. R. (2007). Effect of approach span condition on the vehicle-induced dynamic response of slab-on-girder road bridges. *Engineering Structures*, *29*(12), 3210-3226.

Cantero, D., McGetrick, P., Kim, C. W., & OBrien, E. (2019). Experimental monitoring of bridge frequency evolution during the passage of vehicles with different suspension properties. *Engineering Structures*, pp. *187*, 209–219.

Chen, S. R., & Wu, J. (2010). Dynamic performance simulation of long-span bridge under combined loads of stochastic traffic and wind. *Journal of Bridge Engineering*, *15*(3),219-230.

Chen, S. R., Cai, C. S., & Levitan, M. (2007). Understand and improve the dynamic performance of transportation system—a case study of Luling Bridge. *Engineering structures*, *29*(6), 1043-1051.

Chopra, A.K. (2012). Dynamics of structures, 4th ed. Prentice Hall, New Jersey.

De Roeck, G., Degrande, G., Lombaert, G., & Müller, G. Vehicle-structure interaction effect on the fatigue life of steel orthotropic decks.

Deng, L., & Cai, C. S. (2009). Identification of parameters of vehicles moving on bridges. *Engineering Structures*, *31*(10), 2474-2485.

Deng, L., & Cai, C. S. (2010). Development of dynamic impact factor for performance evaluation of existing multi-girder concrete bridges. *Engineering Structures*, *32*(1), 21- 31.

Deng, L., & Cai, C. S. (2010). Development of dynamic impact factor for performance evaluation of existing multi-girder concrete bridges. *Engineering Structures*, *32*(1), 21- 31.

Deng, L., He, W., & Shao, Y. (2015). Dynamic impact factors for shear and bending moment of supported and continuous concrete girder bridges. *Journal of Bridge Engineering*, *20*(11), 04015005.

Farrar, C. R., & Worden, K. (2010). An introduction to structural health monitoring. *New Trends in Vibration Based Structural Health Monitoring*, 1-17.

Hou, L. Q., Zhao, X. F., Ou, J. P., & Liu, C. C. (2014). A review of nondeterministic methods for structural damage diagnosis. *J. Vib. Shock*, pp. *33*, 50–58.

Huang, D. (2001). Dynamic analysis of steel curved box girder bridges. *Journal of Bridge Engineering*, *6*(6), 506–513.

Huth, O., Feltrin, G., Maeck, J., Kilic, N., & Motavalli, M. (2005). Damage identification using modal data: Experiences on a prestressed concrete bridge. *Journal of Structural Engineering*, *131*(12), 1898-1910.

J.P. Yang, C.Y. Cao, Wheel size embedded two-mass vehicle model for scanning bridge frequencies, Acta Mech. 231 (4) (2020) 1461–1475, doi:10.1007/s00707-019-02595-5.

Kildashti, K., Alamdari, M. M., Kim, C. W., Gao, W., & Samali, B. (2020). Drive-by- bridge inspection for damage identification in a cable-stayed bridge: Numerical investigations. *Engineering structures*, *223*, 110891.

Kocatürk, T., & Şimşek, M. (2006). Vibration of viscoelastic beams subjected to an eccentric compressive force and a concentrated moving harmonic force. *Journal of Sound and Vibration*, *291*(1-2), 302-322.

Law, S. S., & Li, J. (2010). Updating the reliability of a concrete bridge structure based on condition assessment with uncertainties. *Engineering Structures*, *32*(1), 286-296.

Ma, L., Zhang, W., Han, W. S., & Liu, J. X. (2019). Determining the dynamic amplification factor of multi-span continuous box girder bridges in highways using vehicle-bridge interaction analyses. *Engineering Structures*, pp. *181*, 47–59.

Maeck, J. (2003). Damage assessment of civil engineering structures by vibration monitoring.

Múčka, P. (2017). Simulated road profiles according to ISO 8608 in vibration analysis. Journal of Testing and Evaluation, 46(1), 405–418.

OBrien, E., Carey, C., & Keenahan, J. (2015). Bridge damage detection using ambient traffic and moving force identification. *Structural Control and Health Monitoring*, *22*(12), 1396–1407.

Quirke, P., Bowe, C., OBrien, E. J., Cantero, D., Antolin, P., & Goicolea, J. M. (2017). Railway bridge damage detection using vehicle-based inertial measurements and apparent profile. *Engineering structures*, pp. *153*, 421-442.

Sun, Z., Nagayama, T., Nishio, M., & Fujino, Y. (2018). Investigation on a curvature-based damage detection method using displacement under a moving vehicle. *Structural Control and Health Monitoring*, *25*(1), e2044.

Sun, Z., Nagayama, T., Su, D., & Fujino, Y. (2016). A damage detection algorithm utilizing dynamic displacement of the bridge under a moving vehicle. *Shock and Vibration*, *2016*.

Van Khang, N., Dien, N. P., & Van Huong, N. T. (2009). Transverse vibrations of prestressed continuous beams on rigid supports under the action of moving bodies. *Archive of Applied Mechanics*, *79*(10), 939-953.

Xu, Y. L., Zhang, J., Li, J. C., & Xia, Y. (2009). Experimental investigation on statistical moment-based structural damage detection method. *Structural Health Monitoring*, *8*(6), 555-571

Xu, Y. L., Zhang, J., Li, J., & Wang, X. M. (2011). Stochastic damage detection method for building structures with parametric uncertainties. *Journal of sound and vibration*, *330*(20), 4725–4737.

Yang, J. P., & Lee, W. C. (2018). The damping effect of a passing vehicle for indirectly measuring bridge frequencies by EMD technique. *International Journal of Structural Stability and Dynamics*, *18*(01), 1850008.

Yang, Y. B., Li, Y. C., & Chang, K. C. (2014). Constructing the mode shapes of a bridge from a passing vehicle: a theoretical study. *Innovative Structures and Systems*, *13*(5), 797- 819.

Yang, Y. B., Lin, C. W., & Yau, J. D. (2004). Extracting bridge frequencies from the dynamic response of a passing vehicle. *Journal of Sound and Vibration*, *272*(3-5), 471- 493.

Yang, Y. B., Zhang, B., Qian, Y., & Wu, Y. (2018). Contact-point response for modal identification of bridges by a moving test vehicle. *International Journal of Structural Stability and Dynamics*, *18*(05), 1850073.

Yang, Y., Liu, H., Mosalam, K. M., & Huang, S. (2013). An improved direct stiffness calculation method for damage detection of beam structures. *Structural Control and Health Monitoring*, *20*(5), 835-851.

Yang, Y., Mosalam, K. M., Liu, G., & Wang, X. (2016). Damage Detection Using Improved Direct Stiffness Calculations—A Case Study. *International Journal of Structural Stability and Dynamics*, *16*(01), 1640002.

Yang, Y., Yang, Y. B., & Chen, Z. X. (2017). Seismic damage assessment of RC structures under shaking table tests using the modified direct stiffness calculation method. *Engineering Structures*, *131*, 574-586.

Yang, Y., Zhu, Y., Wang, L. L., Jia, B. Y., & Jin, R. (2018). Structural damage identification of bridges from passing test vehicles. *Sensors*, *18*(11), 4035.

Zhu, X. Q., & Law, S. S. (2002). Dynamic load on continuous multi-lane bridge deck from moving vehicles. *Journal of Sound and Vibration*, *251*(4), 697–716.

Rana, S., Adhikary, S., & Tasnim, J. (2022). A statistical index-based damage identification method of a bridge using dynamic displacement under a moving vehicle. Structures, 43, 79–92.

AASHTO, L. (2012). AASHTO LRFD bridge design specifications. *American Association of State Highway and Transportation Officials, Washington, DC*.